Formation Mechanism of Spinel Type Inclusion in 304 Stainless Steel Deoxidized with Ferrosilicon Alloys

Hidekazu Todoroki, Kenji Mizuno, Masato Noda and Takeya Tohge
Technical Research Center, Nippon Yakin Kogyo Co., Ltd.
4-2 Kojimacho, Kawasakiku, Kawasakishi, 210-8558 Japan
Tel.: +81-44-271-3361
Fax.: +81-44-271-3378
e-mail: todoroki@nyk.co.jp

Key words: Spinel, Ferrosilicon, Deoxidation, Stainless steel, Inclusion, Electronic material

INTRODUCTION

A novel technology to control inclusion composition in steel is recently required depending on steel grade, strip thickness and/or surface finishing as well as the pursuit of high cleanliness. In the case of stainless steel, it often is used without surface treatment such as painting due to its excellent corrosion resistance. Therefore, surface quality is of primary importance. It is generally known that existence of hard inclusion such as $MgO \cdot Al_2O_3$ spinel sometimes causes sliver defects on strip surface. Accordingly the formation of spinel inclusion must be avoided.

A number of investigations on deoxidation in molten stainless steel have been so far reported. T. Tohge et al.[1] investigated the deoxidation equilibrium between molten 18Cr-8Ni stainless steel deoxidized by Si and crucible or slag. It was concluded in their study that oxygen potential could be determined depending upon silica activity. T. Fukuyama et al.[2] studied deoxidation products and their deformability with molten 18Cr-8Ni stainless steel deoxidized by Si, Mn and Al. It was demonstrated that Mn-silicate inclusion, which is deformable when hot-rolled, formed with Al content lower than 0.03 wt% and that alumina inclusion which can not be deformed when hot-rolled formed with Al content over 0.04 wt%.

Some studies to clarify the formation mechanism of $MgO \cdot Al_2O_3$ spinel inclusion have been recently reported. H. Itoh et al.[3] studied inclusion compositions in liquid iron in a dolomite crucible deoxidized by Al. It has been revealed that the experimental results well agree with the phase stability diagram of spinel inclusion estimated from thermodynamical data. H. Ohta et al.[4] studied Ca-O and Mg-O equilibria in liquid iron with $CaO\text{-}SiO_2\text{-}Al_2O_3\text{-}MgO$ slags at 1873K using CaO or MgO crucible. In their report the phase stability regions in Fe-Al-Ca-O and Fe-Al-Mg-O systems estimated at 1873K were in good agreement with the experimental data. Some studies performed by T. Nishi[5] and G. Okuyama[6] focused on the effect of slag basicity on MgO content in inclusions in stainless steel resulting in a higher increasing rate of MgO content in inclusions with a higher slag basicity. J. W. Kim et al.[7] reported that $MgO \cdot Al_2O_3$ spinel inclusion in type 304 stainless steel melt deoxidized by Al and Ti could be avoided with a decrease in both of MgO content in an AOD slag and Al content in melt.

It is noted from these previous investigations [3,4,5,6] that a very small amount of Mg and Al (a couple of mass ppm) enables the formation of spinel inclusion in molten iron or steel deoxidized by Al. However, the mechanism of spinel formation, when deoxidized by Si, has not been fully made clear.

In practical operations of type 304 stainless steel using an AOD and/or VOD furnace, most grades are deoxidized by Si except for special use for which extraordinary cleanliness is needed. As the Si source, ferrosilicon is usually used for Cr reduction from a slag phase after decarburization as well as for deoxidation that concurrently goes. It is known that ferrosilicon contains a small amount of impurities such as Al and Ca that is considered to significantly affect deoxidation product. In the present study, the effects of Al and Ca in a ferrosilicon alloy as a deoxidant on inclusion composition were determined to understand how spinel inclusion formed with Si deoxidation.

EXPERIMENTAL DETAILS

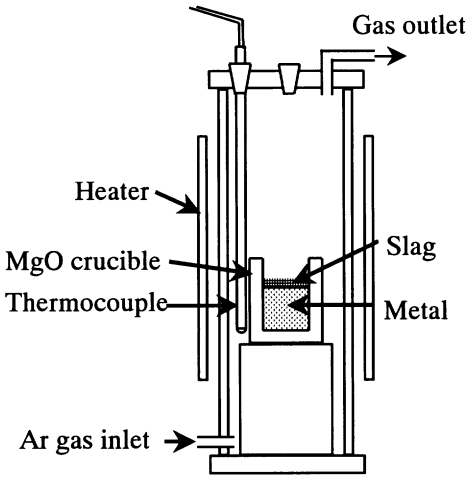

Fig.1. Experimental apparatus.

Table 1 Composition of ferrosilicon alloys (wt%).

	Si	Al	Ca
Type 1	74.9	0.02	<0.01
Type 2	76.0	0.09	<0.01
	75.4	0.44	<0.01
	74.9	1.03	<0.01
	75.4	1.35	<0.01
	76.0	2.91	<0.01
Type 3	76.1	1.71	0.07
	76.1	1.70	0.40
	76.0	1.42	0.84
	76.2	3.31	0.12
	76.4	3.49	0.43
	74.5	2.94	0.90
	75.9	3.00	1.75
Type 4	74.4	0.21	1.70

Table 2 Slag composition (wt%)

CaO	CaF_2	SiO_2	Al_2O_3	MgO
47.6	14.3	28.6	2.8	6.7

Procedure- 500 grams of 18Cr-8Ni stainless steel, which was premelted as a mother metal in an induction furnace without deoxidized, was contained in a MgO crucible and placed in a vertical KERAMAX resistance furnace as shown in Fig. 1. Molten steel was then melted under an Ar gas atmosphere. After the molten steel reached 1823K, the molten steel was sampled followed by an addition of a ferrosilicon alloy and Mn into the molten steel as deoxidants so as to make melt with the composition of 0.5 wt% Si and 1.2 wt% Mn. Various ferrosilicon alloys whose compositions are shown in Table 1 were also premelted prior to experiments as described later in detail. 40 grams of premelted slag whose composition is shown in Table 2 was then added onto the molten steel. Thereafter, molten steel samples were taken at the times of 1, 5, 30, 60, 90 and 120 minutes after deoxidation to analyze chemical compositions and inclusion compositions. The concentrations of Si, Mn, Al, Mg, Ca and O in steel samples were measured by a wet chemical analysis except O by a vacuum fusion method (EMGA-520, HORIBA). Inclusions were analyzed by an EDS method (EMAX-7000, HORIBA). 10 inclusions in a sample were randomly chosen for analysis.

Preparation of ferrosilicon alloys- A variety of ferrosilicon alloys whose compositions are shown in Table 1 were premelted prior to experiments. Si content was basically fixed as 75 wt%. The alloys are classified into 4 types. Namely, type 1 is the ferrosilicon without Al and Ca, type 2 with Al, type 3 with Al and Ca and type 4 with Ca.

The melting procedure is as follows. 75 grams of the mixture of pure iron and silicon was melted at 1643K under an Ar gas atmosphere in an alumina crucible in the furnace same as shown in Fig. 1. Al and Ca were thereafter added into the melt and were mixed stirring by a quartz rod. Then the specimen was taken out to rapidly quench blowing an Ar gas stream. The concentrations of Si, Al, Ca and Mg were measured by a wet chemical analysis. Mg contents were analyzed to be negligibly small so that it was not indicated in Table 1.

RESULTS

Variation of metal compositions- Fig. 2 (a), (b), (c), (d), (e) and (f) show the variations of Si, Mn, Al, Ca, Mg and O contents as time, respectively, after deoxidation with a type 3 ferrosilicon alloy that contains 1.70 wt% Al and 0.40 wt% Ca. Si and Mn contents in the molten steel were constant at 0.5 wt% and 1.2 wt%, respectively, through the experiment. Al rapidly decreased from 0.006 wt% within 30 minutes and then reached the constant values. Ca also has the tendency similar to the behavior of Al. After 60 minutes, plots were placed on the X-axis in convenience because these samples were analyzed to be under analytical limitation. On the other hand, Mg increased up to 0.0002 wt%. The melt contained about 300 ppm of oxygen before deoxidation followed by a rapid decrease after the addition of ferrosilicon. Then it reached the constant values of about 30 ppm after 60 minutes.

Variation of inclusion compositions- Fig. 3 shows the variation of inclusion composition when deoxidized

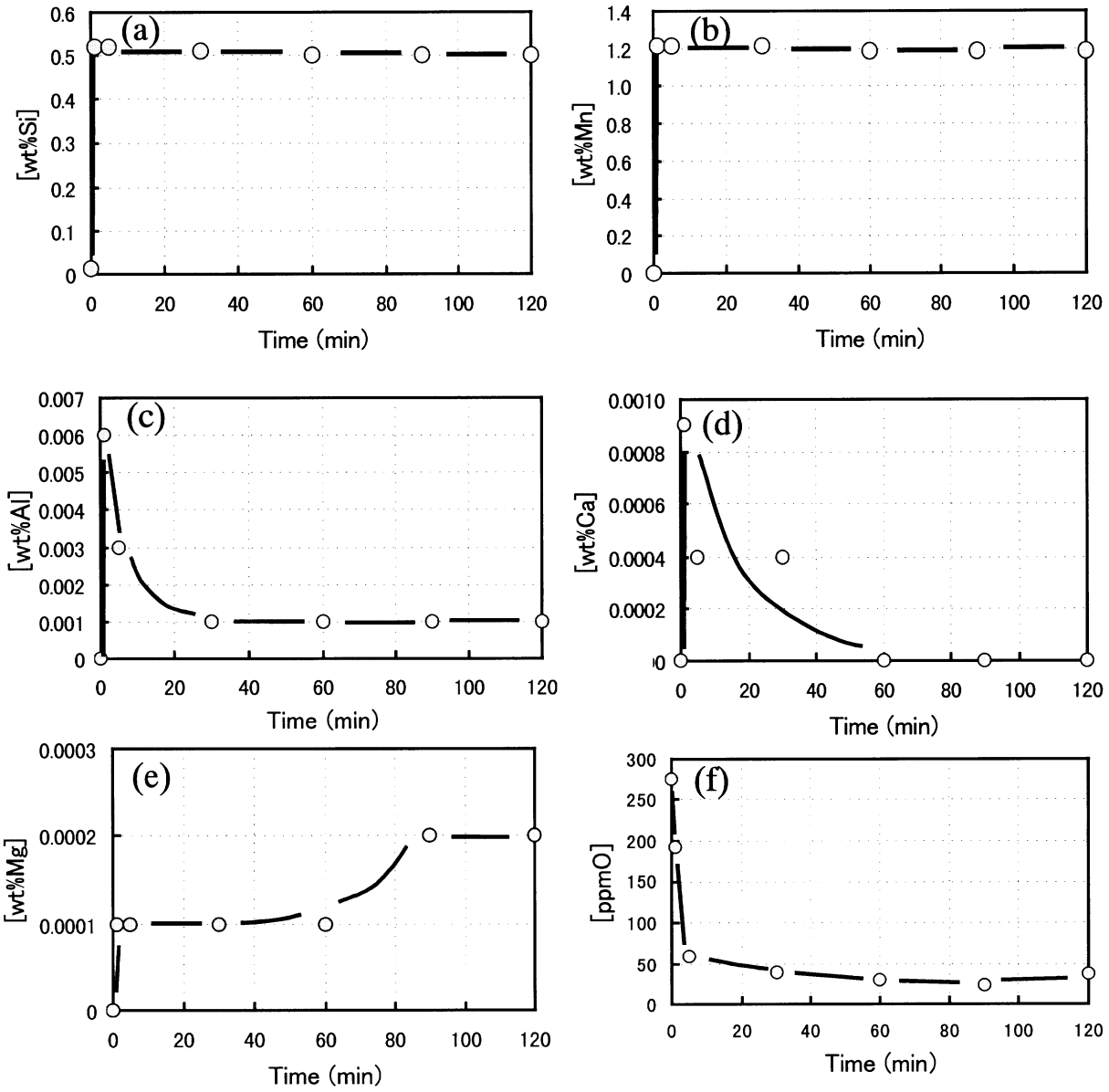

Fig. 2. Variations of metal compositions (a) Si, (b) Mn, (c) Al, (d) Ca, (e)Mg, (f)O. (1.70% Al, 0.40% Ca in type 3 Fe-Si alloy)

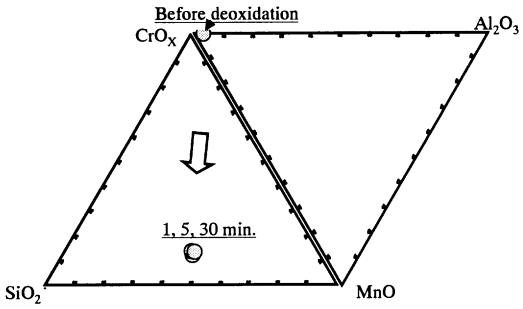

Fig.3. Variation of inclusion composition. (0.02% Al, <0.01% Ca in type 1 Fe-Si alloy)

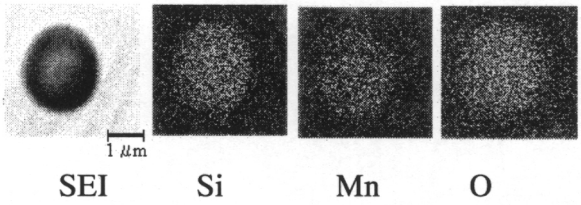

Fig. 4. A typical SiO_2-MnO inclusion analyzed by EDS

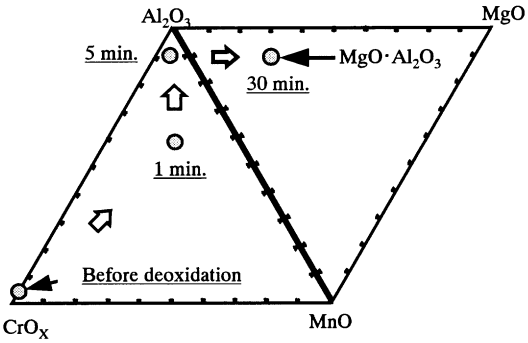

Fig. 5. Variation of inclusion composition. (2.91%Al,<0.01%Ca in type 2 Fe-Si alloy)

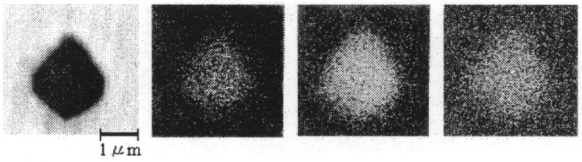

Fig. 6. A typical $MgO \cdot Al_2O_3$ inclusion analyzed by EDS

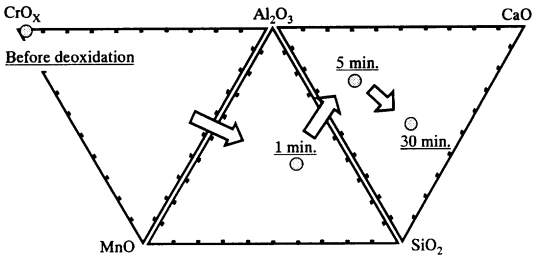

Fig. 7. Variation of inclusion composition. (1.70%Al,0.40%Ca in type 3 Fe-Si alloy)

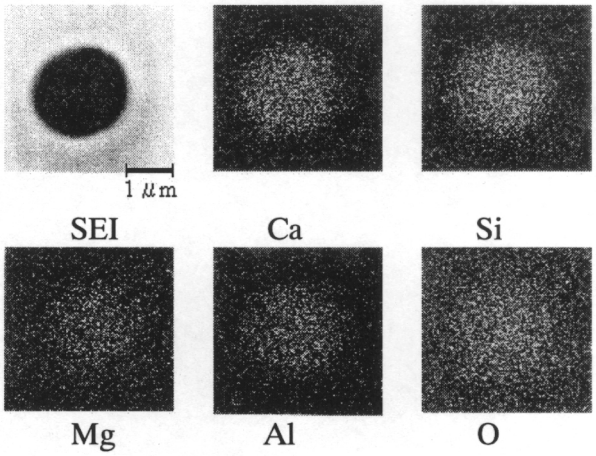

Fig. 8. A typical CaO-SiO_2-MgO-Al_2O_3 inclusion analyzed by EDS

with a type 1 ferrosilicon alloy without both of Al and Ca. As can be seen, inclusion composition is Cr oxide before deoxidation. It was found that in every experiment Cr oxide inclusion formed before adding ferrosilicon. Identification of Cr oxide was not carried out since it was out of focus in this study so that it was indicated as CrO_X in convenience. After the deoxidation MnO-SiO_2 including a small amount of Cr oxide, whose element distribution is shown in Fig. 4, formed and it did not change through the experiment.

Fig. 5 shows the variation of inclusion composition when deoxidized with a type 2 ferrosilicon alloy only with Al (2.91 wt%). Al_2O_3 inclusions formed right after deoxidation. It can be seen that it changed to $MgO \cdot Al_2O_3$ spinel inclusion at 30 minutes after the deoxidation. A typical example of spinel type inclusion is shown in Fig. 6.

Fig. 7 shows the variation of inclusion composition when deoxidized with a type 3 ferrosilicon alloy including 1.70 wt% Al and 0.40 wt% Ca. It can be seen that SiO_2-Al_2O_3-MnO-CaO system complex inclusion formed at 1 minute after deoxidation. However, MnO content gradually

decreased and it finally changed to $CaO\text{-}SiO_2\text{-}Al_2O_3\text{-}MgO$ inclusion, whose element distribution is shown in Fig. 8, at 30 minutes after deoxidation. It was found that the results with the type 4 ferrosilicon alloy including 1.70 wt% Ca showed the tendency same as the experiments with the type 3 ferrosilicon.

As a summary of the results explained above, Fig. 9 shows the compositional region of ferrosilicon alloys where $MgO\cdot Al_2O_3$ spinel inclusion formed at 30 minutes after deoxidation. It is obvious that $MgO\cdot Al_2O_3$ forms when deoxidized with ferrosilicon alloys only with Al over 0.5 wt%.

DISCUSSION

Equilibrium- As shown in Fig. 2 (f) as a typical example, the oxygen content reached the constant values of about 30 ppm after 60 minutes in every experiment. The deoxidation equilibrium with silicon is represented by:

$$SiO_2(s) = \underline{Si} + 2\underline{O}$$

$$\Delta G^\circ = 576{,}440 - 218.2T \qquad (J/mol) \cdots\cdots\cdots\cdots (1)$$

$$K = \frac{a_{Si}\cdot a_O^2}{a_{SiO_2}} = \frac{f_{Si}\cdot[wt\%Si]\cdot f_O^2\cdot[wt\%O]^2}{a_{SiO_2}} \cdots\cdots\cdots\cdots (2)$$

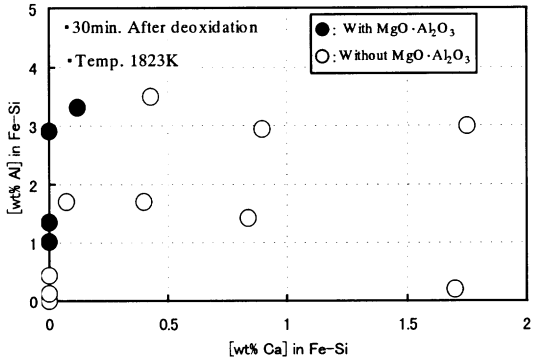

Fig. 9. Compositional region of ferrosilicon alloys where $MgO\cdot Al_2O_3$ spinel forms.

where a_{Si} and a_O are the activities of silicon and oxygen in molten steel relative to a dilute solution of one mass pct standard state and a_{SiO_2} is the activity of silica relative to a pure solid standard state. f_{Si} and f_O are the activity coefficients of silicon and oxygen, respectively, and can be expressed as:

$$\log f_{Si} = e_{Si}^{Si}\cdot[wt\%Si] + e_{Si}^{Mn}\cdot[wt\%Mn] + e_{Si}^{Cr}\cdot[wt\%Cr] + e_{Si}^{Ni}\cdot[wt\%Ni] + e_{Si}^{O}\cdot[wt\%O] + e_{Si}^{Ca}\cdot[wt\%Ca] + e_{Si}^{Al}\cdot[wt\%Al] \qquad \cdots\cdots (3)$$

$$\log f_O = e_O^{Si}\cdot[wt\%Si] + e_O^{Mn}\cdot[wt\%Mn] + e_O^{Cr}\cdot[wt\%Cr] + e_O^{Ni}\cdot[wt\%Ni] + e_O^{O}\cdot[wt\%O] + e_O^{Mg}\cdot[wt\%Mg] + e_O^{Ca}\cdot[wt\%Ca] + e_O^{Al}\cdot[wt\%Al] \cdots\cdots\cdots\cdots (4)$$

where e_i^js are the interaction coefficients given in Table 3 [8,9,10,11]. The thermochemical data used are summarized in Table 4 [4,8,11,12]. a_{SiO_2} can be estimated as 0.005 from the iso-activity lines of $CaO\text{-}SiO_2\text{-}Al_2O_3\text{-}MgO$ system [12] at the composition given in Table 2 assuming that a_{SiO_2} is approximately invariable in this

Table 3 Interaction coefficients e_i^j [8,9,10,11].

i \ j	Si	Mn	Cr	Ni	Mg	Ca	Al	O
Si	0.103	-0.0146	-0.0003	0.005	—	-0.066	0.058	-0.119
Mn	-0.0442	0	0.0039	-0.0072	—	-0.023[10]	—	-0.083
Mg	-0.088	—	0.047[9]	-0.012[11]	—	—	-0.12[9]	-3
Ca	-0.096	-0.007[11]	0.020[11]	-0.044	—	-0.002	-0.072	-1290
Al	0.056	—	0.012[10]	-0.0173[10]	-0.13[9]	-0.047	0.043	-1.98
O	-0.066	-0.021	-0.052	0.006	-1.98	-515	-1.17	-0.20

All data without notation are from Ref. No. 8

study. When the analyzed values of the samples and $a_{SiO_2} = 0.005$ are substituted into Eq.s (2), (3) and (4), oxygen content in equilibrium with silica in the slag phase can be calculated to be 23 ppm. This value is in good agreement with those analyzed (19 to 32 ppm). In fact, it was confirmed that the analytical values of insoluble Al of the samples after 60 minutes were negligibly small. Therefore, most of inclusions that formed in melt could be flown up after 60 minutes of deoxidation. Thus, the discussion about inclusion compositions will be made within 30 minutes of deoxidation because after 60 minutes the observed inclusions may be secondary ones that forms during solidification of the samples.

By the way, the observed inclusion species can be classified into 3 groups depending on the composition as mentioned above. In the following section the mechanism of the formation of each inclusion type will be discussed.

$MnO\text{-}SiO_2$ inclusion (deoxidized by the type 1 ferrosilicon alloys)- $MnO\text{-}SiO_2$ inclusions formed with deoxidation by the type 1 ferrosilicon. Therefore inclusion composition can be determined by the following equations.

$$SiO_2(s) = \underline{Si} + 2\underline{O},$$
$$\Delta G^\circ = 576{,}440 - 218.2T \qquad (J/mol) \cdots\cdots\cdots\cdots (1)$$

$$MnO(s) = \underline{Mn} + \underline{O},$$
$$\Delta G^\circ = 288{,}200 - 129.3T \qquad (J/mol) \cdots\cdots\cdots\cdots (5)$$

The following equation can be deduced from Eq.s (1) and (5),

$$SiO_2(s) + 2\underline{Mn} = \underline{Si} + 2MnO(s),$$
$$\Delta G^\circ = 40 + 40.4T \qquad (J/mol) \qquad \cdots\cdots\cdots\cdots (6)$$

$$K = \frac{a_{Si} \cdot a_{MnO}^2}{a_{Mn}^2 \cdot a_{SiO_2}} = \frac{f_{Si} \cdot [wt\%Si] \cdot a_{MnO}^2}{f_{Mn}^2 \cdot [wt\%Mn]^2 \cdot a_{SiO_2}} \cdots\cdots\cdots\cdots (7)$$

where a_{Si} and a_{Mn} are the activities of silicon and manganese in molten steel relative to a dilute solution of one mass pct standard state and a_{SiO_2} and a_{MnO} are the activities of silica and manganese oxides in inclusion relative to a pure solid standard state. f_{Si} and f_{Mn} are the activity coefficients of silicon and manganese, respectively, and can be expressed as:

Table 4 Thermochemical data.

	ΔG° (J/mol)
$Al_2O_3(s) = 2\underline{Al} + 3\underline{O}$	1,225,000 - 393.8 T [8]
$MgO(s) = \underline{Mg} + \underline{O}$	499,902 - 157.8 T [11]
$SiO_2(s) = \underline{Si} + 2\underline{O}$	576,440 - 218.2 T [8]
$MnO(s) = \underline{Mn} + \underline{O}$	288,200 - 129.3 T [8]
$CaO(s) = \underline{Ca} + \underline{O}$	645,200 - 148.7 T [4]
$MgO \cdot Al_2O_3(s) = Al_2O_3(s) + MgO(s)$	18,828 + 6.3 T [12]

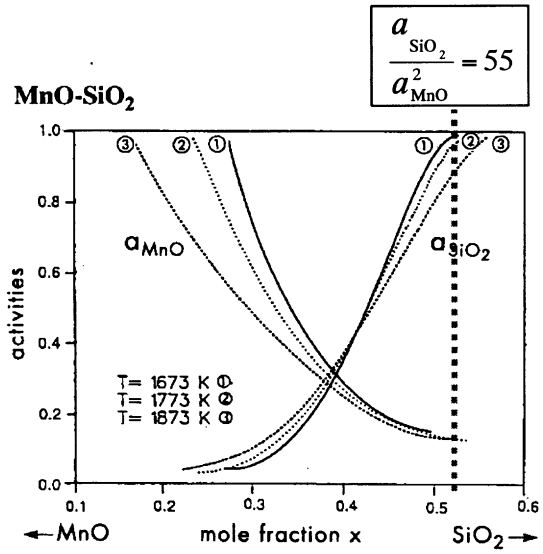

Fig.10. Iso-activity lines for MnO and SiO_2 [13].

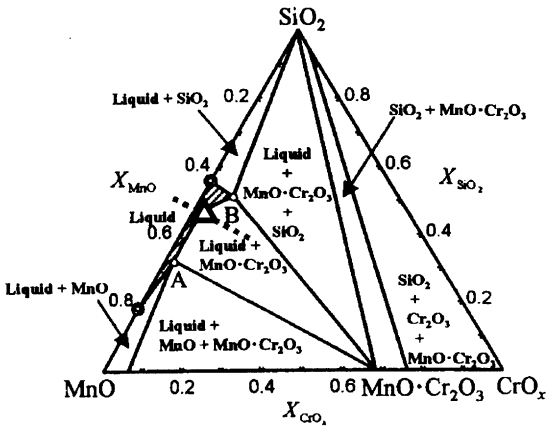

Fig.11. Phase diagram of the $MnO\text{-}SiO_2\text{-}CrO_X$ system [14]. (Po_2/atm=2×10^{-11}, 1873K)
The dashed line shows $a_{SiO_2}/a_{MnO}^2 = 55$. The triangle shows the average composition of the inclusions.

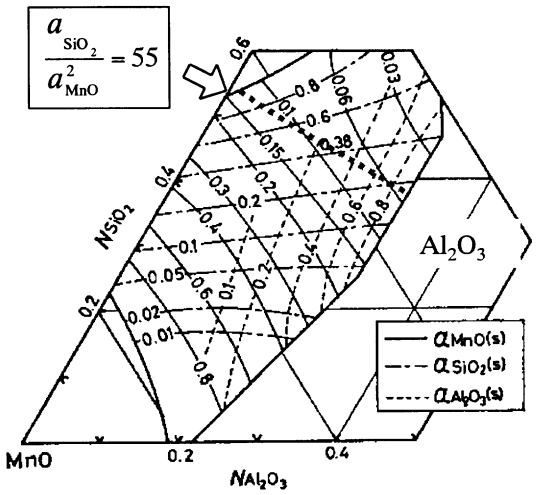

Fig.12. Iso-activity lines for MnO-SiO_2-Al_2O_3 ternary system at 1823K[15].

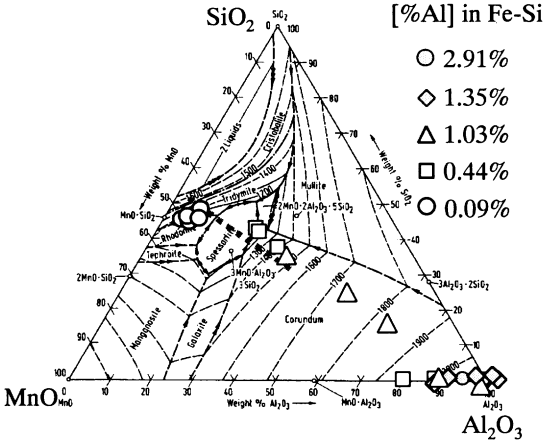

Fig.13. Inclusion compositions at 5min. after deoxidation plotted in SiO_2-MnO-Al_2O_3 system phase diagram[16].

$$\log f_{Si} = e^{Si}_{Si}\cdot[wt\%Si] + e^{Mn}_{Si}\cdot[wt\%Mn] + e^{Cr}_{Si}\cdot[wt\%Cr] + e^{Ni}_{Si}\cdot[wt\%Ni] + e^{O}_{Si}\cdot[wt\%O] + e^{Ca}_{Si}\cdot[wt\%Ca] + e^{Al}_{Si}\cdot[wt\%Al] \quad \cdots\cdots(8)$$

$$\log f_{Mn} = e^{Mn}_{Mn}\cdot[wt\%Mn] + e^{Si}_{Mn}\cdot[wt\%Si] + e^{Cr}_{Mn}\cdot[wt\%Cr] + e^{Ni}_{Mn}\cdot[wt\%Ni] + e^{O}_{Mn}\cdot[wt\%O] + e^{Ca}_{Mn}\cdot[wt\%Ca] \quad \cdots\cdots(9)$$

where e^j_i s are the interaction coefficients given in Table 3. The following relation can be obtained from Eq.s (6), (7), (8) and (9).

$$\frac{a_{SiO_2}}{a^2_{MnO}} = 55 \quad \cdots\cdots(10)$$

Fig. 10 shows the activities of SiO_2 and MnO in SiO_2-MnO binary system [13]. The molecular fraction of SiO_2 corresponds to 0.52 when $a_{SiO_2}/a^2_{MnO} = 55$. Fig. 11 shows the phase diagram of MnO-SiO_2-CrO_X system [14]. A dashed line represents the relation of Eq. (10). A triangle symbol plotted in this figure is the average value of the inclusion compositions from 1 to 30 minutes after deoxidation. As can be seen, the plot well agrees with the line assumed by the thermodynamic data. It should be pointed out that inclusion compositions are affected only by Si and Mn and are independent of the slag phase in the case of the ferrosilicon alloys with no impurity.

$MgO\cdot Al_2O_3$ inclusion (deoxidized by the type 2 ferrosilicon alloys)- At the early stage of deoxidation with the type 2 ferrosilicon alloys, inclusion composition should be determined by the manner same as in the last section because MnO-SiO_2-Al_2O_3 ternary system inclusion formed. Fig. 12 shows the iso-activity lines for MnO, SiO_2 and Al_2O_3 ternary system [15], in which a dashed line shows $a_{SiO_2}/a^2_{MnO} = 55$. Fig. 13 shows the phase diagram of SiO_2-MnO-Al_2O_3 system [16] where the experimental results of 5 minutes after deoxidation are plotted. The plots are located on the dashed line and its extrapolation. It shows that the ratio of MnO/SiO_2 in inclusions can be determined by that of Mn/Si in melt. It can be further realized in Fig. 13 that Al_2O_3 contents in the inclusions increase with increasing Al content in ferrosilicon alloys with keeping the relation of $a_{SiO_2}/a^2_{MnO} = 55$.

As deoxidation goes, $MgO\cdot Al_2O_3$ inclusions formed as shown in Fig. 5. This result implies that the effect of Al as an impurity in a ferrosilicon alloy is significant in the case of Si deoxidation. It is postulated that Mg is transferred from the slag phase by a reducing reaction. It indeed seems that a small amount of Al has the ability to reduce MgO in slag since the reduction of MgO was not seen when adding the type 1 ferrosilicon alloys. Therefore the following reaction may occur:

$$3(MgO)_{in\ Slag} + 2\underline{Al} = (Al_2O_3)_{in\ Slag} + 3\underline{Mg} \quad \cdots(11)$$

Soluble Mg is considered to react with inclusions to form $MgO \cdot Al_2O_3$. So, MgO, $MgO \cdot Al_2O_3$, Al_2O_3 and silicate inclusions in 18Cr-8Ni-0.5Si-1.2Mn melt should be taken into account for an inclusion phase stability diagram that can be obtained from the following reactions:

$$4MgO(s) + 2\underline{Al} = MgO \cdot Al_2O_3(s) + 3\underline{Mg} \quad \cdots(12)$$

$$\Delta G^\circ = 255{,}878 - 85.9T \quad (J/mol)$$

$$K = \frac{a_{MgO \cdot Al_2O_3} \cdot a_{Mg}^3}{a_{MgO}^4 \cdot a_{Al}^2} = \frac{a_{MgO \cdot Al_2O_3} \cdot f_{Mg}^3 \cdot [wt\%Mg]^3}{a_{MgO}^4 \cdot f_{Al}^2 \cdot [wt\%Al]^2} \quad \cdots(13)$$

$$3MgO \cdot Al_2O_3(s) + 2\underline{Al} = 4Al_2O_3(s) + 3\underline{Mg} \quad \cdots(14)$$

$$\Delta G^\circ = 331{,}190 - 60.7 \quad (J/mol)$$

$$K = \frac{a_{Al_2O_3}^4 \cdot a_{Mg}^3}{a_{MgO \cdot Al_2O_3}^3 \cdot a_{Al}^2} = \frac{a_{Al_2O_3}^4 \cdot f_{Mg}^3 \cdot [wt\%Mg]^3}{a_{MgO \cdot Al_2O_3}^3 \cdot f_{Al}^2 \cdot [wt\%Al]^2} \quad \cdots(15)$$

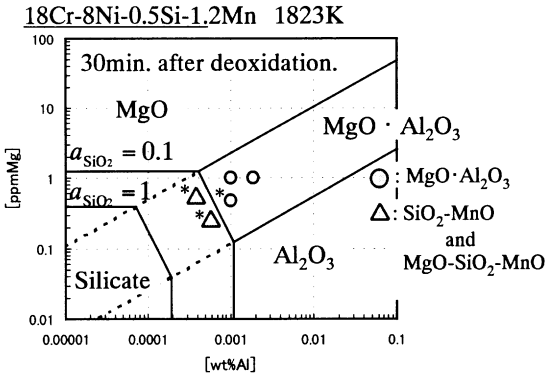

Fig. 14. Phase stability diagram of MgO, $MgO \cdot Al_2O_3$, Al_2O_3 and Silicate inclusions. * under analytical limitation

$$2MgO(s) + \underline{Si} = SiO_2(s) + 2\underline{Mg} \qquad \Delta G^\circ = 423{,}364 - 97.4T \quad (J/mol) \cdots(16)$$

$$K = \frac{a_{SiO_2} \cdot a_{Mg}^2}{a_{MgO}^2 \cdot a_{Si}} = \frac{a_{SiO_2} \cdot f_{Al}^2 \cdot [wt\%Mg]^2}{a_{MgO}^2 \cdot f_{Si} \cdot [wt\%Si]} \quad \cdots(17)$$

$$MgO \cdot Al_2O_3(s) + 2\underline{Si} = 2SiO_2(s) + \underline{Mg} + 2\underline{Al} \qquad \Delta G^\circ = 590{,}850 - 108.9T \quad (J/mol) \cdots(18)$$

$$K = \frac{a_{SiO_2}^2 \cdot a_{Mg} \cdot a_{Al}^2}{a_{MgO \cdot Al_2O_3} \cdot a_{Si}^2} = \frac{a_{SiO_2}^2 \cdot f_{Mg} \cdot [wt\%Mg] \cdot f_{Al}^2 \cdot [wt\%Al]^2}{a_{MgO \cdot Al_2O_3} \cdot f_{Si}^2 \cdot [wt\%Si]^2} \quad \cdots(19)$$

$$2Al_2O_3(s) + 3\underline{Si} = 3SiO_2(s) + 4\underline{Al} \qquad \Delta G^\circ = 720{,}680 - 133.0T \quad (J/mol) \quad \cdots(20)$$

$$K = \frac{a_{SiO_2}^3 \cdot a_{Al}^4}{a_{Al_2O_3}^2 \cdot a_{Si}^3} = \frac{a_{SiO_2}^3 \cdot f_{Al}^4 \cdot [wt\%Al]^4}{a_{Al_2O_3}^2 \cdot f_{Si}^3 \cdot [wt\%Si]^3} \quad \cdots(21)$$

$$\log f_{Al} = e_{Al}^{Si} \cdot [wt\%Si] + e_{Al}^{Cr} \cdot [wt\%Cr] + e_{Al}^{Ni} \cdot [wt\%Ni] \cdots(22)$$

$$\log f_{Mg} = e_{Mg}^{Si} \cdot [wt\%Si] + e_{Mg}^{Cr} \cdot [wt\%Cr] + e_{Mg}^{Ni} \cdot [wt\%Ni] \cdots(23)$$

To describe the boundary between Al_2O_3 and $MgO \cdot Al_2O_3$, the activity of Al_2O_3 should be taken as unity because of no solubility of MgO into Al_2O_3, while that of $MgO \cdot Al_2O_3$ as 0.80 due to the relatively wide range of a solid solution at 1823K according to the MgO-Al_2O_3 phase diagram[16] if assuming an ideal solution. The activities of MgO and $MgO \cdot Al_2O_3$ are taken as 0.99 and unity, respectively, considering the same manner as stated above, to describe the boundary between MgO and $MgO \cdot Al_2O_3$. Fig. 14 shows the phase stability diagram as a function of silica activity drawn for 18Cr-8Ni-0.5Si-1.2Mn melt at 1823 K. The results agree with the estimated phase stability diagram even though some of the experimental data are under analytical limitation. It is apparent in this figure that a very small amount of Al and Mg enables the formation of spinel same as the previous results [3,4,5].

CaO-SiO_2-Al_2O_3-MgO inclusion (deoxidized by the type 3 and 4 ferrosilicon alloys)- Fig. 15 shows the phase diagram of CaO-SiO_2-Al_2O_3 system [16] where the experimental results of 5 minutes after deoxidation are plotted. The plots are located on the line between the $CaO \cdot Al_2O_3 \cdot 2SiO_2$ phase and Al_2O_3. Besides, Al_2O_3 content does not depend on Al content in the ferrosilicon alloys. This reason is not fully understood at this time but the inclusion compositions can be surely determined by Ca, Si and Al that are involved in the type 3 ferrosilicon immediately after deoxidation.

Similarly to the case of the type 2 ferrosilicon alloys, it is postulated that Mg is transferred from the slag phase by reducing reactions. In this case the following reactions may occur:

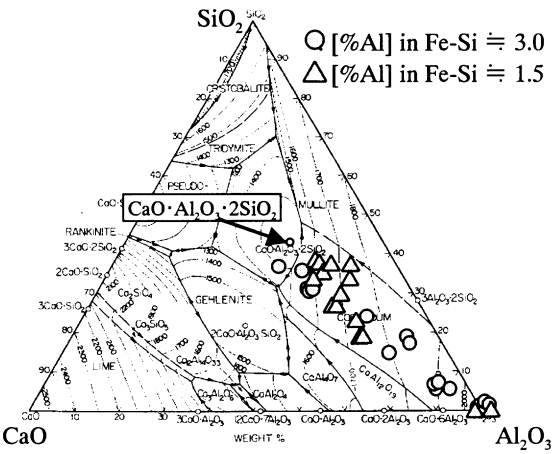

Fig.15. Inclusion compositions at 5min. after deoxidation plotted in CaO-SiO_2-Al_2O_3 system phase diagram[16].

$$3(MgO)_{\text{in Slag}} + 2\underline{Al} = (Al_2O_3)_{\text{in Slag}} + 3\underline{Mg} \quad \cdots(24)$$

$$(MgO)_{\text{in Slag}} + \underline{Ca} = (CaO)_{\text{in Slag}} + \underline{Mg} \quad \cdots(25)$$

It appears that soluble Mg reacts with the inclusions to form CaO-MgO-SiO_2-Al_2O_3 inclusions. In this case, MgO, $MgO \cdot Al_2O_3$, Al_2O_3 and Calcium-silicate inclusions in 18Cr-8Ni-0.5Si-1.2Mn melt should be taken into account for an inclusion phase stability diagram that can be obtained by the manner same as calculated in the last section. Because the type 3 ferrosilicon alloys contain Ca, Ca content in melt has to be considered for a calculation. Calcium content in melt can be obtained by the following reaction:

$$CaO(s) = \underline{Ca} + \underline{O} \qquad \Delta G^\circ = 645{,}200 - 148.7T \quad (J/mol) \quad \cdots(26)$$

$$K = \frac{a_{Ca} \cdot a_O}{a_{CaO}} = \frac{f_{Ca} \cdot [wt\%Ca] \cdot f_O \cdot [wt\%O]}{a_{CaO}} \quad \cdots(27)$$

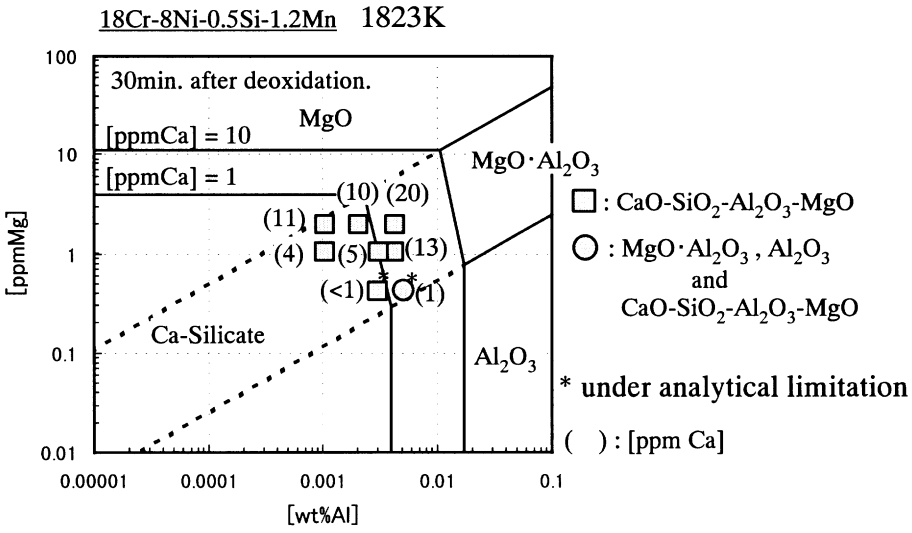

Fig. 16. Phase stability diagram of MgO, $MgO \cdot Al_2O_3$, Al_2O_3 and Ca-Silicate inclusions.

where the activity of CaO, whose standard state is a pure solid, in Calcium-silicate inclusion saturated with MgO and Al_2O_3 is estimated from the activity of CaO in $CaO-SiO_2-MgO$ and $CaO-SiO_2-Al_2O_3$ systems [12], respectively. Fig. 16 shows the phase stability diagram as a function of the calcium content in melt drawn for 18Cr-8Ni-0.5Si-1.2Mn melt at 1823 K. It can be seen that the experimental results agree with the phase stability diagram. It should be noticed that the point of the solid circle, where Ca-silicate, $MgO \cdot Al_2O_3$ and Al_2O_3 formed, is located very close to the point where three boundary lines cross when the Ca content is 1 mass ppm though the Mg content was under analytical limitation. This implies that the calculation is valid enough to predict an inclusion composition. It should be further noted that Ca significantly widens the region of Ca-silicate inclusion. This tendency is in good agreement with that by H. Itoh [3]. The discussion about the type 4 ferrosilicon alloys was omitted here because the tendency was quite similar to that of the type 3 ferrosilicon alloys.

As a summary of this study, Fig. 17 shows a schematic illustration of slag-metal-inclusion-refractory reactions that are considered to take place in this system. At first, $CaO-SiO_2-Al_2O_3$ inclusions form when a ferrosilicon alloy with Al and Ca is added. A small amount of soluble Al and Ca reacts with slag and refractory to transfer Mg from slag to metal phase. The reaction with slag should be more significant comparing with that with refractory due to its faster diffusion rate. The reaction between soluble Mg and inclusions thereafter takes place to form $CaO-MgO-SiO_2-Al_2O_3$ inclusions. In the case of lack of Ca in ferrosilicon alloy, spinel inclusion is more stable than silicate type as shown in Fig. 14. When a ferrosilicon alloy does not contain both Al and Ca, $MnO-SiO_2$ inclusions that form immediately after deoxidation do not change due to no ability to reduce MgO in slag.

Therefore, the addition of ferrosilicon alloy with Ca is one of the countermeasures to prevent spinel formation from the point of view of ferrosilicon alloys for Si deoxidation because silicate inclusions in general do not form large clusters owing to their lower melting temperatures than spinel. Another way is to use very pure ferrosilicon alloy with no impurity. However, it seems not to be realistic in various aspects for practical operations.

This technology can be of course applied for the grades other than type 304 stainless steels. In particular, high cleanliness is required for electronic materials such as Fe-36Ni and Fe-42Ni alloys. For these alloys inclusions larger than 5 μm in a thin sheet significantly affect their properties of punching and etching [17]. The application of this technology enables the control of inclusion composition to be silicate with relatively low melting temperature. Silicate inclusions can be elongated when hot-rolled and become harmless after cold-rolled because they are broken into tiny pieces. Therefore we recently apply this technology for these alloys and good results are continuously obtained.

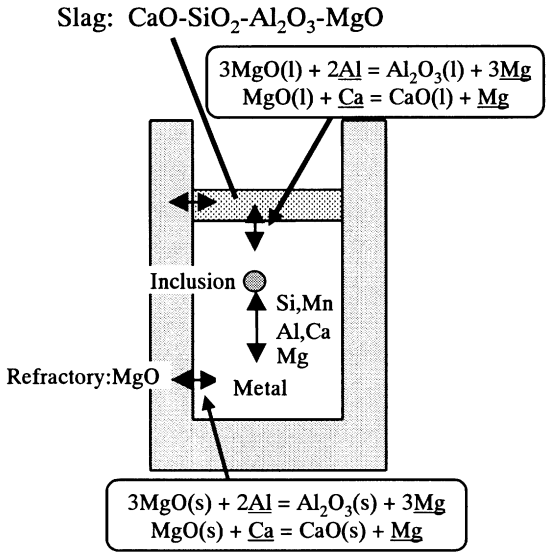

Fig. 17. Schematic illustration of slag-matal-inclusion-refractoy reactions.

CONCLUSIONS

In order to understand the effects of Al and Ca in ferrosilicon alloys on inclusion composition, deoxidation experiments were undertaken. The following conclusions summarize the study:

(1) Immediately after deoxidation, the inclusion compositions were determined only by the elements involved in the ferrosilicon alloys.
(2) The inclusion compositions changed as time with the significant influence of slag-metal reaction.

(3) Al in ferrosilicon alloys was found to reduce MgO in slag phase to enhance the formation of spinel inclusion.
(4) Ca in ferrosilicon alloys was found to prevent the formation of spinel inclusion to form silicate inclusion with relatively low melting temperature.
(5) The phase stability diagram calculated from the thermodynamical data well agreed with the measured inclusion compositions at the last stage of deoxidation.

REFERENCES

1) T. Tohge and T. Watanabe: Trans. ISIJ., 15 (1975) 580-588.
2) T. Fukuyama and K. Segawa: Tetsu-to-Hagane, 55 (1969) 139-144.
3) H. Itoh, M. Hino and S. Ban-ya: Tetsu-to-Hagane, 84 (1998) 98-90.
4) H. Ohta and H. Suito: Metall. Trans. B, 28B (1997) 1131-1139.
5) T. Nishi and K. Shimme: Tetsu-to-Hagane, 84 (1998) 837-843.
6) G. Okuyama, S. Takeuti and K. Sorimati: CAMP-ISIJ, 10 (1997) 847.
7) J. W. Kim, K. S. Kim, D. S. Kim, D. Y. Lee and K. P. Yang: ISIJ Int., 36 (1996) S140-S143.
8) Recommended Values of Equilibrium Constants for the Reactions in Steelmaking, Japan Society for the Promotion of Science, 19th Committee, Tokyo, (1984).
9) Q. Han: Proc. of 6th Int. Iron Steel Congress, Vol. 1, ISIJ, Tokyo, I, (1990), 166.
10) H. Ohta and H. Suito: ISIJ Int., 36 (1996), 983
11) M. Nadif and C. Gatellier: Process Technology Proc. 5th. ISS. (1986), 741
12) H. R. Rein and J. Chipman: Trans. Met. Soc. AIME, 233, (1965), 415
13) B. Rao and D. R. Gaskell: Met. Trans. 12B, (1981), 311
14) T. Fujisawa et al. : Japan Society for the Promotion of Science, Reaction Process Division, 19th Committee, (1999), Report No. II -37
15) T. Fujisawa and H. Sakao: Tetsu-to-Hagane, 63 (1977) 1494-1503.
16) M. Allibert et al. : SLAG ATLAS 2nd Edition ed. by VDEh, (1995)
17) A. W. Cramb: Scand. J. Metall., Suppl. 26 (1997), 2-7